

Quantum Hardware-in-the-Loop for Optimal Power Flow in Renewable-Integrated Power Systems

Zeynab Kaseb, *Student Member IEEE*, Rahul Rane, *Student Member IEEE*,
Aleksandra Lekić, *Senior Member IEEE*, Matthias Möller, Amin Khodaei, *Senior Member IEEE*,
Peter Palensky, *Senior Member IEEE*, and Pedro P. Vergara, *Senior Member IEEE*

Abstract—This paper presents a proof-of-concept for integrating quantum hardware with real-time digital simulator (RTDS) to model and control modern power systems, including renewable energy resources. Power flow (PF) analysis and optimal power flow (OPF) studies are conducted using RTDS coupled with Fujitsu's CMOS Digital Annealer and D-Wave's Advantage™ quantum processors. The adiabatic quantum power flow (AQPF) and adiabatic quantum optimal power flow (AQOPF) algorithms are used to perform PF and OPF, respectively, on quantum and quantum-inspired hardware. The experiments are performed on the IEEE 9-bus test system and a modified version that includes solar and wind farms. The findings demonstrate that the AQPF and AQOPF algorithms can accurately perform PF and OPF, yielding results that closely match those of classical Newton-Raphson (NR) solvers while also exhibiting robust convergence. Furthermore, the integration of renewable energy sources (RES) within the AQOPF framework proves effective in maintaining system stability and performance, even under variable generation conditions. These findings highlight the potential of quantum computing to significantly enhance the modeling and control of future power grids, particularly in systems with high renewable energy penetration.

Index Terms—Adiabatic quantum computing, combinatorial optimization, state estimation, load flow, real-time simulation.

I. INTRODUCTION

The global transition toward sustainable energy has driven a rapid expansion of renewable energy sources (RES), particularly photovoltaic (PV) solar and wind farms. However, the inherent intermittency and stochastic behavior of these resources pose significant challenges to power system operation, thus requiring advanced methodologies to ensure stability and reliability [1]. On the other hand, the rising costs and environmental impact of fossil fuels have underscored the urgency of minimizing their use and integrating RES more effectively [2].

To maintain secure and efficient grid operation, transmission and distribution system operators (TSOs and DSOs), rely on power flow (PF) analysis to assess system conditions [3].

Zeynab Kaseb, Rahul Rane, Aleksandra Lekić, Peter Palensky, and Pedro P. Vergara are associated with the Intelligent Electrical Power Grids Section, Electrical Sustainable Energy, Delft University of Technology, The Netherlands.

Matthias Möller is associated with the Delft Institute of Applied Mathematics, Delft University of Technology, The Netherlands.

Amin Khodaei is associated with Electrical and Computer Engineering, University of Denver.

Corresponding author: Zeynab Kaseb. Email: Z.Kaseb@tudelft.nl

This work is part of the DATALESS project 482.20.602, which is jointly financed by the Dutch Organization for Scientific Research (NWO), and National Natural Science Foundation of China (NSFC).

When economic, stability, or operational objectives must be optimized, this extends to the optimal power flow (OPF) problem. OPF, therefore, plays a crucial role in power system operation and planning by determining the most efficient system configuration through the adjustment of control variables, including active and reactive power dispatch, transformer tap positions, and reactive power compensation [4]. By solving OPF problems, system operators can minimize generation costs, enhance voltage stability, and ensure compliance with operational constraints, thereby improving the overall efficiency and cost-effectiveness of modern power systems [5].

Classical OPF models, including linear programming (LP) (e.g., [6]), nonlinear programming (NLP) (e.g., [7]), quadratic programming (QP) (e.g., [8]), and Newton-based approaches (e.g., [9]), have been extensively studied and widely adopted in both academia and industry [10]. While these solvers have proven effective for traditional power systems, their application to modern RES-integrated systems presents significant challenges. The inherent intermittency and uncertainty of RES introduce complex, large-scale, and highly nonlinear optimization problems, often leading to slow convergence and excessive computational burden in classical OPF solvers [11]. As a result, advanced OPF algorithms are needed to efficiently handle non-convexity, scale effectively for real-time applications, and account for the stochastic nature of RES while ensuring system stability and optimal operation [12].

Recent research has explored artificial intelligence (AI) techniques as promising alternatives. These approaches employ data-driven models to enhance scalability, improve convergence speed, and enable real-time decision-making in complex power systems. Deep learning models, including physics-informed neural networks (PINNs) (e.g., [3], [13]), have been employed to embed power system physics into AI algorithms to ensure solutions remain physically consistent while accelerating OPF computations. Similarly, graph neural networks (GNNs) (e.g., [14]) have been applied to exploit the underlying topological structure of power systems, which allows for efficient and scalable OPF approximations. Reinforcement learning (RL) (e.g., [15]) has also gained attention for its ability to iteratively learn optimal control policies, adapting dynamically to real-time power system conditions.

Despite the advancements brought by AI in OPF solutions, significant challenges remain unresolved. AI-based approaches, while accelerating OPF computations, often rely on extensive training datasets and may suffer from generalization issues when encountering unseen grid conditions. Further-

more, their ability to guarantee feasibility and adherence to power system physics is constrained, necessitating hybrid approaches that still depend on conventional solvers. Moreover, the non-convex, large-scale nature of OPF problems continues to pose computational challenges that classical and AI-based approaches struggle to address in real-time applications (e.g., [16], [17]).

In this perspective, quantum computing has emerged as an alternative approach to address the OPF problem by offering the potential for accelerated computation and improved solution accuracy. Quantum computing can be broadly classified into two paradigms: gate-based quantum computing (GQC) and adiabatic quantum computing (AQC). While GQC has gained significant attention due to advancements in quantum circuit design and error mitigation techniques (e.g., [18], [19]), its practical application to OPF problems remains challenging. This is primarily due to its dependence on large-scale, fault-tolerant hardware and its sensitivity to noise, which degrades computational accuracy and limits its effectiveness in solving large-scale OPF problems (e.g., [20]–[24]). Recent studies have attempted to implement GQC for power system problems, such as [25], which explores quantum circuit-based methods for OPF, and [26], which investigates quantum-enhanced DC-OPF problem. However, these approaches still face scalability and feasibility issues, considering the aforementioned bottleneck regarding GQC.

In contrast, AQC exhibits better noise resilience and has demonstrated promising results for combinatorial optimization problems, which makes it a promising candidate for OPF problems. Quantum annealing is particularly well-suited for optimization problems that can be formulated as Ising models or quadratic unconstrained binary optimization (QUBO) problems. The work in [27] provides a comprehensive overview of the theoretical foundations and practical implementations of quantum annealing, highlighting its advantages in solving NP-hard optimization problems. More specifically, research such as [28] has explored the application of quantum annealing to the unit commitment problem, which shares structural similarities with OPF. Similarly, [29] investigates the effectiveness of quantum annealing for higher-order Ising models, which could be used to enhance the efficiency of OPF problems.

Despite these promising developments, research on employing AQC for OPF remains in its early stages. Some initial efforts, such as [30], have explored quantum algorithms tailored for OPF, but challenges persist in mapping the full AC-OPF problem onto quantum annealing hardware. Other studies, such as [28], [31], demonstrate the feasibility of AQC in power system optimization. Comparative studies suggest that while AQC offers advantages in solving constrained optimization problems efficiently on quantum hardware, further advancements in problem formulation, embedding techniques, and quantum hardware capabilities are required for practical deployment in real-time power system operations [29].

From the deployment perspective, practical validation of quantum algorithms for power system operations is crucial for evaluating their feasibility, performance, and scalability in real-world applications. While theoretical advances in quantum optimization indicate great potential [32], testing under re-

alistic operating environments is required to identify practical limitations and challenges. Hardware-in-the-loop (HIL) simulation is an effective approach for such evaluations because it can integrate physical hardware, such as quantum processors, with real-time power system simulations. HIL provides a controlled yet realistic testing environment in which quantum algorithms' performance, stability, and responsiveness can be systematically tested under dynamic settings, such as variable renewable energy generation, changing load demands, and grid disturbances (e.g., [33], [34]).

In this context, a Quantum-in-the-Loop (QIL) framework, which integrates GQC with real-time power system simulations, has the potential to address complex optimization challenges in modern smart grids [35]. For example, the QIL framework presented in [35] emphasizes using quantum mechanics to enhance grid operations by processing inputs from numerous distributed sensors and controllers. However, as previously noted, GQC currently faces significant challenges, including noise and limited practical implementation [21].

This paper presents a novel Quantum Hardware-in-the-loop (QHIL) framework for addressing the OPF problem in power systems with high renewable energy integration, where the computational strengths of Fujitsu's CMOS Digital Annealer and D-Wave's Advantage™ quantum computing system are used to solve the OPF problem building on the formulation presented in [32]. Further, these quantum computing platforms are interfaced with RTDS® real-time simulator, which can accurately model and simulate real-time power system dynamics. The proposed framework is validated using the IEEE 9-bus test system with integrated solar and wind farms as a proof-of-concept. The results demonstrate that quantum optimization is feasible and effective in real-time power system operations. The main contributions of this paper are listed below:

- A QHIL framework is developed that seamlessly integrates a real-time digital simulator (RTDS) with Fujitsu's CMOS Digital Annealer and D-Wave's Advantage™ quantum computing system to solve OPF problems.
- A Windows-based middleware is implemented that enables efficient and reliable communication between Fujitsu's Digital Annealer and the RTDS to ensure real-time compatibility.
- The feasibility of integrating RTDS with quantum hardware in a QHIL environment is demonstrated through a rigorous proof-of-concept, which achieves predefined accuracy thresholds and validates the potential for practical deployment in power system optimization.

II. MATHEMATICAL FORMULATION

In a power system comprising N buses, the relationship between the complex bus voltages \mathbf{V} and complex bus currents \mathbf{I} is described by Ohm's Law in matrix form, as given in:

$$\mathbf{I} = \mathbf{Y}\mathbf{V}, \quad \mathbf{I}, \mathbf{V} \in \mathbb{R}^N, \quad \mathbf{Y} \in \mathbb{R}^{N \times N} \quad (1)$$

where \mathbf{Y} is the complex bus admittance matrix. Each element of the admittance matrix is expressed as:

$$Y_{ik} = G_{ik} + jB_{ik}, \quad \forall i, k \in \{1, \dots, N\}, \quad (2)$$

where G_{ik} and B_{ik} represent the conductance and susceptance between buses i and k , respectively. Further, the net complex power flowing through the network can be given by:

$$\mathbf{S} = \mathbf{V}\mathbf{I}^* = \mathbf{V} \circ (\mathbf{Y}\mathbf{V})^*, \quad (3)$$

where $\mathbf{S} = \mathbf{P} + j\mathbf{Q}$ represents a complex power injection vector, \circ denotes element-wise vector multiplication, and $*$ denotes the complex conjugation operation. The power flowing through bus i can also be expressed as the difference between the total generation power and the total demand power, as:

$$S_i = S_i^G - S_i^D, \forall i \in \{1, \dots, N\}, \quad (4)$$

where S_i denotes the net power flowing through bus i , S_i^G and S_i^D represent the total power generated and total power demand at bus i , respectively. Expanding (4) into its real and imaginary components yields:

$$P_i + jQ_i = (P_i^G - P_i^D) + j(Q_i^G - Q_i^D), \quad \forall i \in \{1, \dots, N\}, \quad (5)$$

Here, P_i and Q_i are net active and reactive power injections, respectively; P_i^G and Q_i^G are total generated active and reactive power, respectively; and P_i^D and Q_i^D are total demand active and reactive power, respectively.

P_i and Q_i can also be expressed in terms of voltage and admittance parameters by combining and simplifying (2), (3) and (5), yielding:

$$P_i + jQ_i = \mathbf{V}_i \sum_{k=1}^N \mathbf{Y}_{ik} \mathbf{V}_k, \quad \forall i, k \in \{1, \dots, N\}. \quad (6)$$

Further expanding (6) into real and imaginary components yields:

$$P_i = \sum_{j=1}^N G_{ij}(\mu_i \mu_j + \omega_i \omega_j) + B_{ij}(\omega_i \mu_j - \mu_i \omega_j), \quad (7a)$$

$$Q_i = \sum_{j=1}^N G_{ij}(\omega_i \mu_j - \mu_i \omega_j) - B_{ij}(\mu_i \mu_j + \omega_i \omega_j), \quad (7b)$$

where μ_i and ω_i are the real and imaginary parts of the complex voltage at bus i , respectively.

A. Classical PF

The objective of PF analysis is to compute the bus voltages and power injections that satisfy the power balance equations, as given in:

$$P_i = P_i^G - P_i^D, \quad \forall i \in \{1, \dots, N\}, \quad (8a)$$

$$Q_i = Q_i^G - Q_i^D, \quad \forall i \in \{1, \dots, N\}. \quad (8b)$$

These equations must be solved iteratively, typically using numerical methods such as the Newton-Raphson (NR) or Gauss-Seidel algorithms.

B. Classical OPF

The OPF problem aims to compute the optimal generator outputs $\{P_i^G, Q_i^G\}$ that minimize generation costs while satisfying all system constraints, i.e. the power balance, generation, and operational limits. The problem can be formulated as:

$$\min \sum_{k \in \mathbb{G}} f_k(P_k^G) \quad (9)$$

subject to:

$$P_i = P_i^G - P_i^D \quad (10a)$$

$$Q_i = Q_i^G - Q_i^D \quad (10b)$$

$$\underline{P_i^G} \leq P_i^G \leq \overline{P_i^G} \quad (10c)$$

$$\underline{Q_i^G} \leq Q_i^G \leq \overline{Q_i^G} \quad (10d)$$

$$\underline{V_i} \leq V_i \leq \overline{V_i} \quad (10e)$$

$$\underline{\delta_i} \leq \delta_i \leq \overline{\delta_i} \quad (10f)$$

Here, $f_k(\cdot)$ is the generator's fuel cost function. \mathbb{G} is a subset of buses connected to generators $\{1, 2, \dots, N_G\}$, where N_G is the total number of generators. $\underline{P_i^G}$ and $\overline{P_i^G}$ represent the minimum and maximum limits for the generated active power at bus i , respectively. $\underline{Q_i^G}$ and $\overline{Q_i^G}$ are the minimum and maximum limits for the generated reactive power at bus i , respectively. $\underline{V_i}$ and $\overline{V_i}$ denote the minimum and maximum limits for the voltage magnitudes at bus i , respectively. Finally, $\underline{\delta_i}$ and $\overline{\delta_i}$ represent the minimum and maximum limits for the voltage phase angles at bus i , respectively.

C. Adiabatic Quantum Power Flow (AQPF)

Solving (8) with the aid of quantum and/or quantum-inspired (digital) annealers amounts to minimizing the sum of all the terms squared as given in:

$$H_{\text{obj}}(\mathbf{x}) = \sum_{i=1}^N (P_i - P_i^G + P_i^D)^2 + (Q_i - Q_i^G + Q_i^D)^2, \quad (11)$$

where \mathbf{x} represents vectors of binary variables. To convert the problem into a form that quantum and/or digital annealers can solve, (7) is expanded into:

$$P_i = \sum_{j=1}^N \mu_i G_{ij} \mu_j + \omega_i G_{ij} \omega_j + \omega_i B_{ij} \mu_j - \mu_i B_{ij} \omega_j, \quad (12a)$$

$$Q_i = \sum_{j=1}^N \omega_i G_{ij} \mu_j - \mu_i G_{ij} \omega_j - \mu_i B_{ij} \mu_j - \omega_i B_{ij} \omega_j. \quad (12b)$$

D. Adiabatic Quantum Optimal Power Flow (AQOPF)

The classical OPF problem is restructured and reformulated into a problem Hamiltonian that can be solved using quantum and digital annealers. It is composed of the objective term, H_{obj} , as defined in (11), along with the inequality constraint terms, H_{const} , and the quality constraint term, H_{cost} , as defined in (13) and (14), respectively.

The inequality constraints of the classical OPF problem, i.e., (10c) to (10f), are integrated into the problem Hamiltonian as penalty terms. A typical penalty term for an inequality

constraint $g(x) \leq 0$ is $\lambda \max(0, g(x))^2$, where λ is a penalty parameter. This results in (13) for the adiabatic quantum OPF formulation to ensure that the active and reactive power generation limits, voltage limits, and angle limits are respected by penalizing any violations.

$$\begin{aligned}
H_{\text{const}}(\mathbf{x}) = & \sum_{i \in \mathbb{G}} \left[\lambda_0 \max(0, P_i^G - \overline{P_i^G})^2 \right. \\
& + \lambda_1 \max(0, \underline{P_i^G} - P_i^G)^2 \\
& + \lambda_2 \max(0, Q_i^G - \overline{Q_i^G})^2 \\
& \left. + \lambda_3 \max(0, \underline{Q_i^G} - Q_i^G)^2 \right] \\
& + \sum_{i=1}^N \left[\lambda_4 \max(0, V_i - \overline{V_i})^2 \right. \\
& + \lambda_5 \max(0, \underline{V_i} - V_i)^2 \\
& + \lambda_6 \max(0, \delta_i - \overline{\delta_i})^2 \\
& \left. + \lambda_7 \max(0, \underline{\delta_i} - \delta_i)^2 \right]. \tag{13}
\end{aligned}$$

Finally, the objective of the classical OPF problem (9) needs to be incorporated into the problem Hamiltonian as a penalty term. A typical penalty term for an equality constraint is $\lambda h(x)^2$, where λ is a penalty parameter and $h(x) = 0$ is the equality constraint. This results in:

$$H_{\text{cost}}(\mathbf{x}) = \lambda_8 \sum_{k \in \mathbb{G}} f_k(P_k^G)^2 \tag{14}$$

Combining the objective and constraints Hamiltonian gives:

$$H(\mathbf{x}) = H_{\text{obj}}(\mathbf{x}) + H_{\text{const}}(\mathbf{x}) + H_{\text{cost}}(\mathbf{x}) \tag{15}$$

It should be noted that while the penalty-based formulation presented in (13) and (14) allows for encoding constraints within the problem Hamiltonian, practical implementation in available quantum/digital computing platforms, such as PyQUBO and DADK, presents challenges. Specifically, these platforms do not natively support the use of the $\max(\cdot)$ function, nor can they directly enforce inequality conditions. To address this limitation, slack binary variables need to be introduced to enable the conversion of these constraints into a form suitable for binary encoding and ensure compatibility with quantum/digital annealers.

E. Quadratic Unconstrained Binary Optimization (QUBO)

A QUBO formulation is defined by a symmetric, real-valued matrix $\mathbf{Q} \in \mathbb{R}^{n \times n}$ and the binary minimization problem:

$$\min_{\vec{x} \in \{0,1\}^N} f_{\mathbf{Q}}(\vec{x}) \tag{16}$$

with the quadratic objective function given by:

$$f_{\mathbf{Q}}(\vec{x}) = \vec{x}^T \mathbf{Q} \vec{x} = \sum_{i=1}^N \sum_{j=1}^N Q_{ij} x_i x_j \tag{17}$$

A straightforward discretization of μ_i and ω_i in (12) is:

$$\mu_i = \mu_i^0 + x_{i,0}^\mu \Delta \mu_i - x_{i,1}^\mu \Delta \mu_i, \tag{18a}$$

Algorithm 1 Adiabatic quantum algorithm for PF analysis.

```

1: Initialize  $\mathbf{P}^G = [P_1^G, P_2^G, \dots, P_{N_G}^G]$ 
2: Initialize  $\mathbf{P}^D = [P_1^D, P_2^D, \dots, P_{N-N_G-1}^D]$ 
3: Initialize  $\mathbf{Q}^D = [Q_1^D, Q_2^D, \dots, Q_{N-N_G-1}^D]$ 
4: Initialize  $\mathbf{Y} = \{(G_{ij} + jB_{ij}) : i, j = 1, 2, \dots, N\}$ 
5:  $\Delta \mu \leftarrow 1 \times 10^{-2}$ 
6:  $\Delta \omega \leftarrow 1 \times 10^{-3}$ 
7:  $\mu^0 = [\mu_1^0, \mu_2^0, \dots, \mu_N^0] \leftarrow 1$ 
8:  $\omega^0 = [\omega_1^0, \omega_2^0, \dots, \omega_N^0] \leftarrow 0$ 
9: Calculate  $\mathbf{P} = [P_2, P_3, \dots, P_N]$  using (12a)
10: Calculate  $\mathbf{Q} = [Q_2, Q_3, \dots, Q_N]$  using (12b)
11: Calculate Hamiltonian  $H_{\text{obj}}(\mathbf{x})$  using (11)
12:  $\epsilon \leftarrow 1 \times 10^{-2}$ 
13:  $\text{it} \leftarrow 0$ 
14: while  $H_{\text{obj}}(\mathbf{x}) > \epsilon$  and  $\text{it} < \text{it}_{\text{max}}$  do
15:   Update  $\mathbf{x}$ 
16:   Update  $\mu$  and  $\omega$  using (18)
17:   Recalculate  $\mathbf{P}$  using (12a)
18:   Recalculate  $\mathbf{Q}$  using (12b)
19:   Recalculate  $H_{\text{obj}}(\mathbf{x})$  using (11)
20:   Update  $\mu^0$  and  $\omega^0$ 
21:   Update  $\Delta \mu, \Delta \omega$ 
22:    $\text{it} \leftarrow \text{it} + 1$ 
23: end while

```

$$\omega_i = \omega_i^0 + x_{i,0}^\omega \Delta \omega_i - x_{i,1}^\omega \Delta \omega_i, \tag{18b}$$

where $x_{i,\{0,1\}}^{\{\mu,\omega\}} \in \{0,1\}$ are binary decision variables whose value decides whether the base values μ_i^0 and ω_i^0 are increased ($x_{i,0} = 1 \wedge x_{i,1} = 0$), decreased ($x_{i,0} = 0 \wedge x_{i,1} = 1$), or kept at their current value ($x_{i,0} = 0 \wedge x_{i,1} = 0$ or $x_{i,0} = 1 \wedge x_{i,1} = 1$).

F. Implementation of Adiabatic Quantum Algorithms

Working out all the terms at (11) for AQPF and (15) for AQOPF yields a fourth-order polynomial for the binary variables. Detailed information on the expanded formulations is available in [32]. The solvers are Fujitsu's Quantum-Inspired Integrated Optimization software (QIIO) and D-Wave's Advantage™ system (QA). The former can efficiently handle higher-order terms. The latter, however, can handle only quadratic terms, and, hence, higher-order terms need to be reduced to at most quadratic ones by introducing auxiliary variables. A possible approach is to introduce auxiliary variables of the form $z_{ij} = x_i x_j$ and replace triplet interactions by:

$$x_i x_j x_k = \min_{z_{ij}} \{z_{ij} x_k + \lambda P(x_i, x_j; z_{ij})\}, \quad \lambda > 0 \tag{19}$$

with:

$$P(x_i, x_j; z_{ij}) = x_i x_j - 2(x_i + x_j)z_{ij} + 3z_{ij}, \tag{20}$$

Expressions with four binary variables can be replaced by:

$$x_i x_j x_k x_l = \min_{z_{ij}, z_{kl}} \{\lambda P(x_i, x_j; z_{ij}) + \lambda P(x_k, x_l; z_{kl})\}. \tag{21}$$

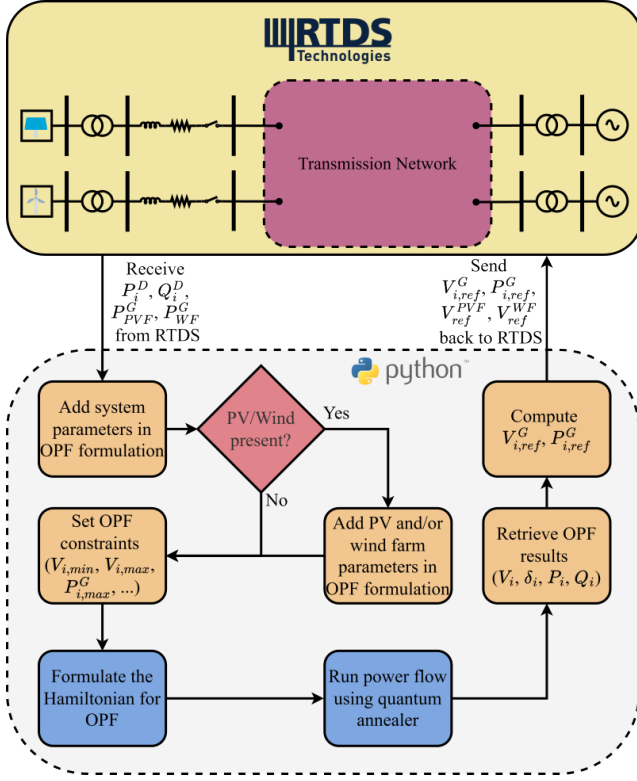


Fig. 1. Computational and information flow within the QHIL framework for OPF calculations. The OPF formulation receives system parameters, real-time data (e.g., P_i^D , Q_i^D , P_i^{PVF} , P_i^{WFF}), and operational constraints. The AQOPF algorithm solves the OPF using a problem Hamiltonian on quantum/digital annealers, and the results are compared to the classical NR method using Pandapower solver. The computed generator set points ($V_{i,ref}^G$, $P_{i,ref}^G$) are then employed in the real-time power system simulation.

The Python package PyQUBO is used in this study to develop the QUBO based on (11) for PF and (15) for OPF when the solver is QA to reduce higher-order terms. Once the minimization problem (11) and (15) is solved, the resulting bitstring can be used to update μ_i and ω_i according to (18a) and (18b), respectively. Note that the auxiliary z_{ij} variables for the voltage updates are neglected. For all solvers, the number of readouts is 5000. Algorithm 1 represents the pseudo-code to perform AQPF and AQOPF using quantum/digital annealers. A detailed description of the algorithm can be found in [32].

III. QUANTUM HARDWARE-IN-THE-LOOP FRAMEWORK

This section provides an overview of the proposed QHIL framework, shown in Fig. 1, which deploys real-time power system simulations conducted with RTDS coupled with Fujitsu's CMOS digital annealer quantum computing system and D-Wave's Advantage™ system.

A. Computational and Information Flow

Fig. 1 depicts the computational and information flow within the QHIL framework for the OPF calculation. The OPF problem formulation is initially given essential system parameters such as the number of buses (N), system connectivity, and transmission line resistance, inductance, and capacitance, as

well as real-time data from the simulator, such as demand power values (P_i^D , Q_i^D) and RES power generation outputs (P_i^{PVF} , P_i^{WFF}). If solar and/or wind farms are included in the system, their parameters are also added. Furthermore, several OPF constraints, such as bus voltage (\underline{V}_i , \overline{V}_i) and generation limits (\underline{P}_i^G , \overline{P}_i^G , \underline{Q}_i^G , \overline{Q}_i^G), are provided to ensure that the power system functions within acceptable operating limits.

The OPF problem (9) and (10) is then solved using the AQOPF algorithm. This approach converts the OPF problem into a Hamiltonian representation (15) that can be executed by quantum and digital annealers. The results are subsequently collected from the annealers. The output values are used to calculate the required generator voltage ($V_{i,ref}^G$) and active power ($P_{i,ref}^G$) set points based on the approach used for modeling the generator's excitor and governor in the real-time power system simulation. The required generator voltage ($V_{i,ref}^G$) set point is given by:

$$V_{i,ref}^G = \frac{E_{f,i,pu}^G}{K_a} + V_{i,pu}^G \quad (22a)$$

$$\bar{E}_{f,i,pu}^G = \bar{V}_{i,pu}^G + jx_d \bar{I}_{i,pu}^G \quad (22b)$$

$$\bar{I}_{i,pu}^G = \frac{S_{i,pu}^*}{\bar{V}_{i,pu}^G} \quad (22c)$$

$$S_{i,pu} = \frac{P_i^G + jQ_i^G}{S_{base}} \quad (22d)$$

where K_a is the excitor gain, x_d represents the d -axis reactance of the generator, $\bar{E}_{f,i,pu}^G$ is the field voltage of the generator in per-unit, $\bar{I}_{i,pu}^G$ is the current flowing through the generator in per-unit, $\bar{V}_{i,pu}^G$ is the generator terminal voltage, $S_{i,pu}$ is the apparent power supplied by the generator in per-unit, and S_{base} represents the base MVA value. Similarly, the generator's active power ($P_{i,ref}^G$) set point can be computed using:

$$P_{i,ref}^G = R \frac{P_i^G}{S_{base}} \quad (23)$$

where R is the governor droop coefficient. Finally, the estimated generator and RES converter set points ($V_{i,ref}^G$, $P_{i,ref}^G$, $V_{i,ref}^{PVF}$, $V_{i,ref}^{WFF}$) are returned to the simulator as input for system operation.

B. Hardware Configuration

Fig. 2 illustrates the hardware configuration of the QHIL framework proposed in this paper. Power system simulations are carried out on the RTDS® NovaCor racks and its response can be monitored using RSCAD, which provides a user-friendly interface. To provide real-time connectivity with the simulator, an external communication GTNETx2 card is used which, when configured with the card's SKT protocol, allows the simulator and external devices to communicate via transmission control protocol (TCP). This TCP communication allows the simulator to export valuable system parameters, such as power demand values (P_i^D , Q_i^D) and RES power generation (P_i^{PVF} , P_i^{WFF}), as inputs to the OPF algorithm. Here, P_i^{PVF} and P_i^{WFF} represent the active power generated by the PV and wind farms, respectively. Subsequently, the computed generator and RES converter set points ($V_{i,ref}^G$,

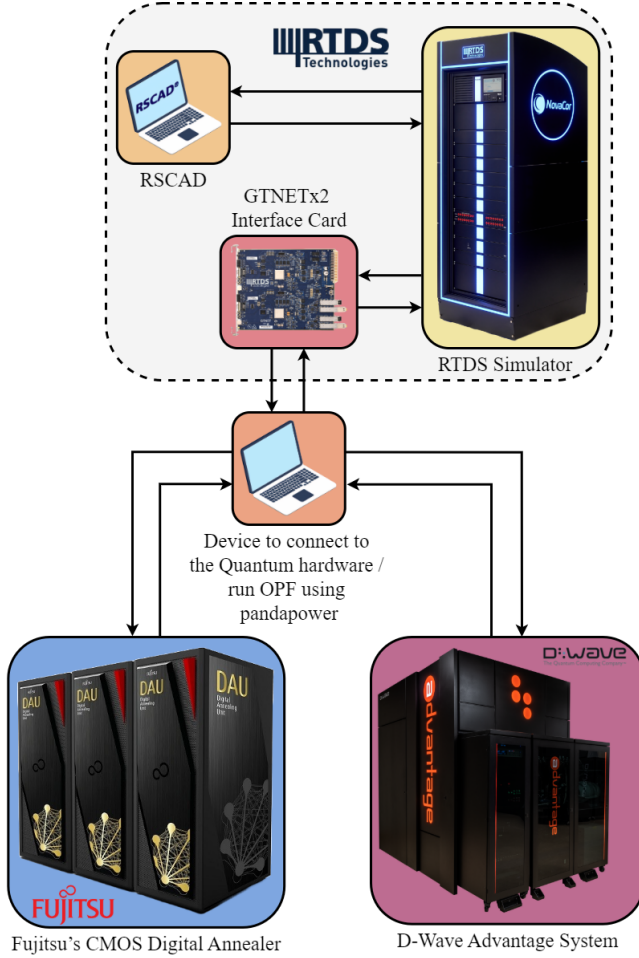


Fig. 2. Hardware configuration of the proposed QHIL framework for real-time power system simulations using RTDS® and RSCAD. A GTNETx2 card with SKT protocol enables TCP communication to exchange system parameters and RES generation data with the OPF algorithm running on the quantum hardware or local device, which then returns generator and converter set points to the simulator in real time.

$P_{i,ref}^G$, $V_{i,ref}^{PVF}$, $V_{i,ref}^{WVF}$) are sent back to the simulator in real-time.

The RTDS can be directly interfaced with D-Wave’s quantum annealer. However, a direct connection with Fujitsu’s CMOS digital annealer is currently not feasible, primarily due to the lack of proximity between hardware and the simulation environment and, secondly, because vendor-specific VPN network access is required. Therefore, a Windows-based system serves as an intermediate to facilitate communication between Fujitsu’s digital annealer and the RTDS.

The inputs required for the OPF algorithm are sent via Python scripts to the AQOPF algorithm. This algorithm is executed within a Windows Subsystem for Linux (WSL) environment running a virtual Ubuntu instance, where the required Python packages (e.g., dwave, pyqubo, dadk) are installed. Azure VPN Client is used to establish a connection with Fujitsu’s digital annealer. However, this step is not necessary for D-Wave’s quantum annealer. After the AQOPF algorithm computes the OPF solution, the corresponding generator set points are then transmitted back to the simulation loop. Note

TABLE I
GENERATOR PARAMETERS FOR THE IEEE 9-BUS TEST SYSTEM WITH INTEGRATED RES, INCLUDING GENERATOR LOCATIONS, CAPACITIES, AND OPERATIONAL LIMITS.

Sr. No.	Bus i	P_i^G (MW)	V_i (p.u.)	δ_i (deg.)	\bar{P}_i^G (MW)	\underline{P}_i^G (MW)	\bar{Q}_i^G (MVAR)	\underline{Q}_i^G (MVAR)
1	1	-	1	0	250	10	300	-300
2	2	163	1	-	300	10	300	-300
3	3	85	1	-	270	10	300	-300
4	11	19.8	1	-	19.8	19.8	20	-20
5	13	19.8	1	-	19.8	19.8	20	-20

that the D-Wave Advantage™ system has over 5,000 qubits and 35,000 couplers for encoding the problem Hamiltonian, while Fujitsu’s digital annealer V5 has up to 100,000 qubits organized in units of 8,192 fully-connected qubits and operates with 64-bit precision.

IV. RESULTS

The results of applying the AQPF and AQOPF algorithms to the IEEE 9-bus test system are presented. First, the test system used for evaluation is described, followed by the configuration of the quantum and digital annealers employed in the experiments. Finally, the performance of the AQPF and AQOPF algorithms is analyzed, and their effectiveness across different hardware platforms is compared.

A. Modeling of the Test Power System

The IEEE 9-bus system is a simplified representation of a power grid, with nine buses, three generators, three transformers, and six transmission lines, as depicted in Fig. 3. Three of the buses are categorized as *PV* buses, indicating generators that provide active power and regulate the bus voltage by controlling the reactive power. These generators are connected to buses 1, 2, and 3. The remaining six buses are *PQ* buses, which may or may not be connected to a load. Specifically, loads are connected to buses 5, 7, and 9. Three step-up transformers connect the generators to the transmission network, and six transmission lines interconnect the buses.

A 1 MW solar and a 2.5 MW wind farm have been modeled and connected to bus 7 to integrate RES, as shown in Fig. 3. These farms are then scaled up to 20 MW each, using the sub-step scaling option available when modeling in RTDS®. Each RES is connected to the power system via a step-up transformer and a series *RL* branch, ensuring that the farms’ short circuit ratio remains constant as power output varies. A switch is also included to allow for the connection and disconnection of the RES when simulating various operational conditions. Since these RES units are equipped with voltage controllers at their respective connecting buses, they can be effectively modeled as *PV* buses in the PF and OPF formulations. Tables I to IV respectively summarize the test system’s generator, load, line, and cost parameters, considering base values of 345 kV and 100 MVA.

B. Annealer Configuration

The computational setup for solving PF and OPF problems using AQC is detailed in Table V. Table VI presents results

TABLE V
PERFORMANCE COMPARISON OF DIFFERENT ANNEALERS FOR THE AQPF AND AQOPF ALGORITHMS IN TERMS OF VARIABLE COUNT, COMPILATION TIME, AND ITERATION TIME ACROSS VARIOUS TEST SYSTEMS.

Test System	Algorithm	Annealer	Compiler	Var. No.	Compile Time (s)	It. Time (s)	It. No.
9-bus	AQPF	QA	PyQUBO	666	4.35	238.48	152
9-bus	AQPF	QIIO	DADK	249	0.27	0.93	119
9-bus	AQOPF	QIIO	DADK	331	0.42	1.81	200
13-bus	AQOPF	QIIO	DADK	635	41.25	42.37	200

TABLE VI
DEVIATION ANALYSIS OF VOLTAGE MAGNITUDE (V_i), PHASE ANGLE (δ_i), ACTIVE POWER (P_i), AND REACTIVE POWER (Q_i) FOR AQPF AND AQOPF ALGORITHMS USING DIFFERENT ANNEALERS ACROSS TEST SYSTEMS.

Test System	Algorithm	Annealer	$ \Delta V_i $ (p.u.)	$\sigma_{ \Delta V_i }$ (p.u.)	$ \Delta \delta_i $ (deg.)	$\sigma_{ \Delta \delta_i }$ (deg.)	$ \Delta P_i $ (MW)	$\sigma_{ \Delta P_i }$ (MW)	$ \Delta Q_i $ (MVAR)	$\sigma_{ \Delta Q_i }$ (MVAR)
9-bus	AQPF	QA	2.53×10^{-4}	2.41×10^{-4}	2.13×10^{-3}	1.37×10^{-3}	0.03	0.04	0.18	0.29
9-bus	AQPF	QIIO	1.29×10^{-3}	1.64×10^{-3}	1.88×10^{-2}	2.15×10^{-2}	0.47	0.76	0.86	1.85
9-bus	AQOPF	QIIO	1.43×10^{-3}	2.67×10^{-3}	7.82×10^{-2}	8.60×10^{-2}	0.09	0.26	0.14	0.36
13-bus	AQOPF	QIIO	1.57×10^{-3}	9.83×10^{-4}	1.52×10^{-2}	2.20×10^{-2}	0.06	0.16	1.13	2.84

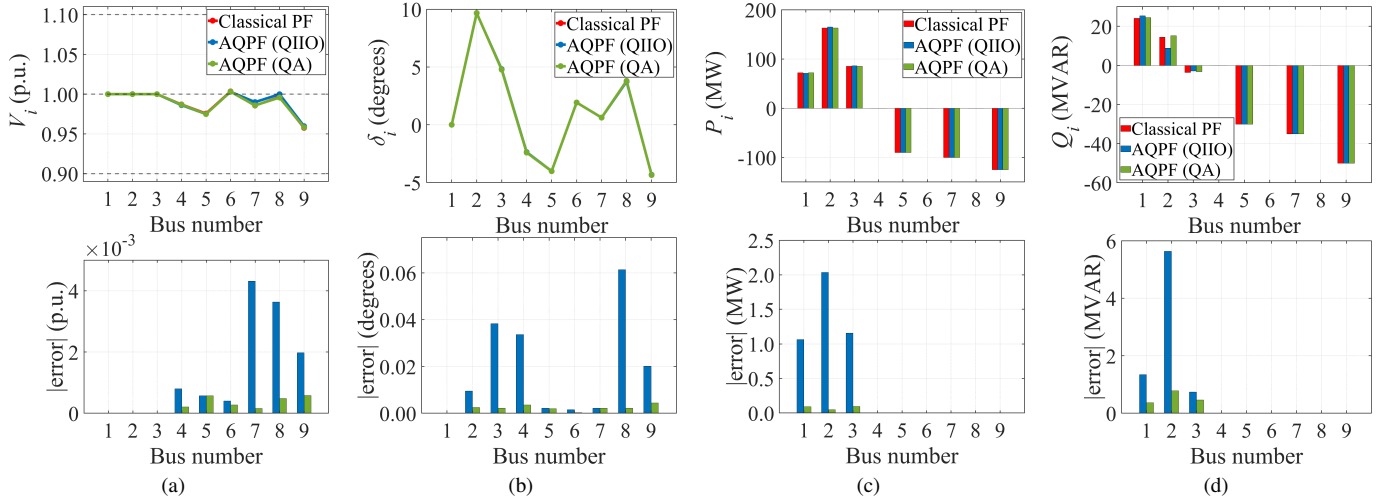


Fig. 4. PF results for the IEEE 9-bus system using the AQPF algorithm on QA and QIIO, compared to the classical NR method. The top row shows the computed values for (a) bus voltage magnitude (V_i), (b) phase angle (δ_i), (c) active power (P_i), and (d) reactive power (Q_i). The bottom row illustrates the absolute errors between the quantum solvers (QA and QIIO) and the NR benchmark for each corresponding parameter.

the effectiveness of the AQOPF approach in handling OPF problems in both conventional and renewable-integrated power systems. The mean deviation in voltage magnitude between AQOPF and NR remains within the predefined error threshold of 1×10^{-2} (Fig. 6a). The mean difference in voltage phase angle is 0.02 degrees (Fig. 6b). The mean deviations in net active and reactive power are 6.92×10^{-2} MW and 1.15 MVAR, respectively (Figs. 6c and 6d).

V. DISCUSSION

The following observations can be made:

- The integration with quantum hardware provides a novel means of solving PF and OPF problems efficiently, which can offer potential speedup as quantum computers continue to improve compared to classical methods.
- For real-time power system applications, computational efficiency is crucial. While current quantum hardware limitations prevent immediate deployment, future ad-

vancements in quantum processors may enable real-time optimization for power system control and stability analysis.

- While the approach is promising, scalability remains a challenge. Larger power systems require more qubits and, hence, are more time-consuming.

VI. CONCLUSION

In this paper, a quantum hardware-in-the-loop framework is proposed. Quantum annealing algorithms, namely the adiabatic quantum power flow (AQPF) and adiabatic quantum optimal power flow (AQOPF) algorithms are used to perform OPF. The experiments are performed based on the IEEE 9-bus test system and a modified version of it where renewable energy sources are integrated. The quantum annealing algorithm is coupled with the RTDS environment to perform real-time simulations.

The results demonstrate the effectiveness of the quantum annealing algorithms in solving PF and OPF problems us-

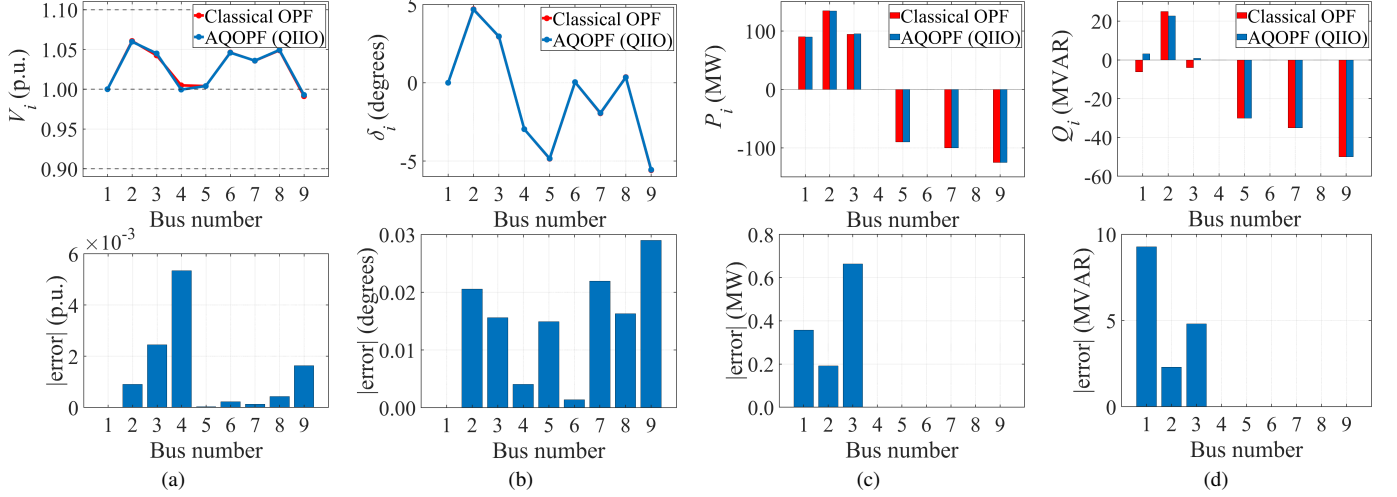


Fig. 5. OPF results for the IEEE 9-bus system using the AQOPF algorithm on QIIO, compared to the classical NR method. The top row shows the computed values for (a) bus voltage magnitude (V_i), (b) phase angle (δ_i), (c) active power (P_i), and (d) reactive power (Q_i). The bottom row illustrates the absolute errors between the quantum solver (QIIO) and the NR benchmark for each corresponding parameter.

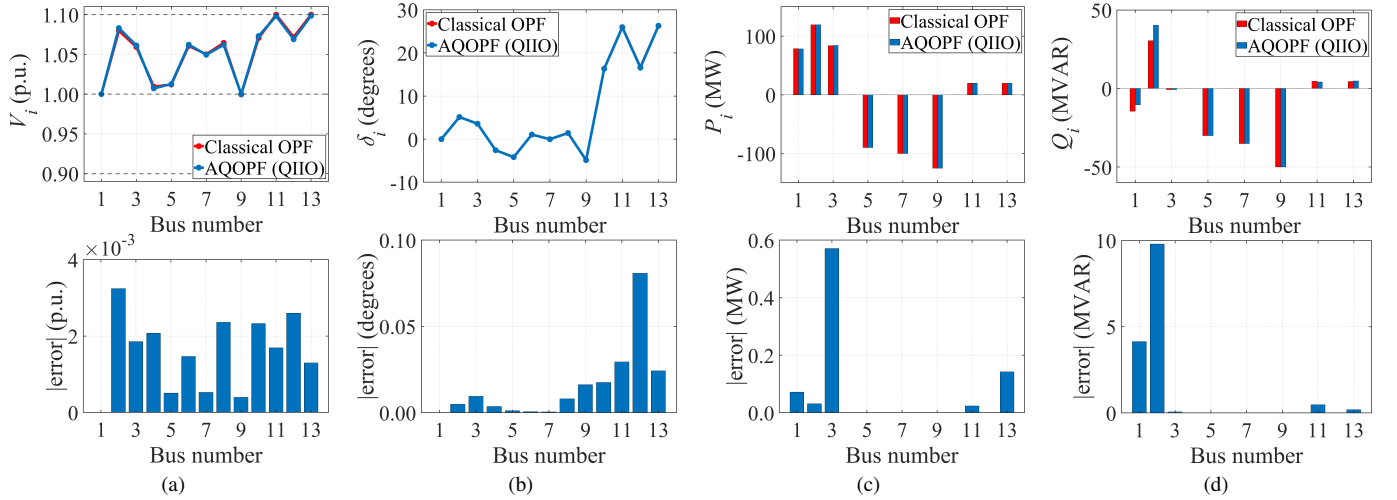


Fig. 6. OPF results for the IEEE 9-bus system with integrated RES using the AQOPF algorithm on QIIO, compared to the classical NR method. The top row shows the computed values for (a) bus voltage magnitude (V_i), (b) phase angle (δ_i), (c) active power (P_i), and (d) reactive power (Q_i). The bottom row illustrates the absolute errors between the quantum solver (QIIO) and the NR benchmark for each corresponding parameter.

ing quantum hardware. The experiments confirm that both Fujitsu's Quantum-Inspired Integrated Optimization software (QIIO) and D-Wave's Advantage™ system (QA) produce solutions with high accuracy, closely aligning with classical NR benchmarks. QA exhibits superior performance in net active and reactive power calculations, achieving up to 90% accuracy improvement over QIIO.

Scalability tests validate the robustness of AQOPF in handling both conventional and renewable-integrated power systems. The algorithm maintains minimal deviations in voltage magnitude, phase angle, and power values while integrating large-scale RES, demonstrating its potential for real-world applications. The renewable-integrated IEEE 9-bus test case confirms that AQOPF effectively accommodates RES variability while preserving grid stability.

These findings highlight the promise of quantum computing in power system analysis, which paves the way for future

research on large-scale grid applications. The demonstrated accuracy, scalability, and adaptability of AQPF and AQOPF underscore their potential to enhance PF and OPF computations, particularly in renewable-dominated networks, and hence make a significant step toward quantum-enhanced energy management solutions.

ACKNOWLEDGMENT

The authors extend their sincere gratitude to Jülich Supercomputing Centre for providing computing time on the D-Wave Advantage™ System JUPSI through the Jülich Unified Infrastructure for Quantum computing (JUNIQU). The research received support from the Center of Excellence RAISE, which receives funding from the European Union's Horizon 2020–Research and Innovation Framework Programme H2020-INFRAEDI-2019-1 under grant agreement no. 951733.

The authors also like to thank Fujitsu Technology Solutions for providing access to the QIO software¹ and, in particular, to Markus Kirsch and Matthieu Parizy for their support and custom extensions of the DADK Python package. Furthermore, the authors acknowledge the invaluable support of lab technician Remko Koornneef for his assistance in setting up the RTDS laboratory and facilitating hardware communication and integration, which greatly contributed to the successful completion of the experimental work.

REFERENCES

- [1] M. S. Alam, F. S. Al-Ismael, A. Salem, and M. A. Abido, "High-level penetration of renewable energy sources into grid utility: Challenges and solutions," *IEEE access*, vol. 8, pp. 190 277–190 299, 2020.
- [2] H. van Asselt, P. Fragkos, L. Peterson, and K. Fragkiadakis, "The environmental and economic effects of international cooperation on restricting fossil fuel supply," *International Environmental Agreements: Politics, Law and Economics*, vol. 24, no. 1, pp. 141–166, 2024.
- [3] Z. Kaseb, S. Orfanoudakis, P. P. Vergara, and P. Palensky, "Adaptive informed deep neural networks for power flow analysis," *arXiv preprint arXiv:2412.02659*, 2024.
- [4] M. Huneault and F. D. Galiana, "A survey of the optimal power flow literature," *IEEE Transactions on Power Systems*, vol. 6, no. 2, pp. 762–770, 1991.
- [5] N. Mbuli and W. Ngaha, "A survey of big bang big crunch optimisation in power systems," *Renewable and Sustainable Energy Reviews*, vol. 155, p. 111848, 2022.
- [6] S. Mhanna and P. Mancarella, "An exact sequential linear programming algorithm for the optimal power flow problem," *IEEE Transactions on Power Systems*, vol. 37, no. 1, pp. 666–679, 2021.
- [7] J. A. Momoh, R. Adapa, and M. El-Hawary, "A review of selected optimal power flow literature to 1993. i. nonlinear and quadratic programming approaches," *IEEE Transactions on Power Systems*, vol. 14, no. 1, pp. 96–104, 1999.
- [8] P. Fortenbacher and T. Demiray, "Linear/quadratic programming-based optimal power flow using linear power flow and absolute loss approximations," *International Journal of Electrical Power & Energy Systems*, vol. 107, pp. 680–689, 2019.
- [9] D. N. d. Silva, B. R. Pereira Júnior, and G. R. M. d. Costa, "A novel milp-newton approach for power flow analysis," *IET Generation, Transmission & Distribution*, vol. 15, no. 3, pp. 518–532, 2021.
- [10] A. F. Zobaa, S. A. Aleem, and A. Y. Abdelaziz, *Classical and recent aspects of power system optimization*. Academic Press, 2018.
- [11] A. Ali, A. Hassan, M. Keerio, N. H. Mugheri, G. Abbas, M. Hatatah, E. Touti, and A. Yousef, "A novel solution to optimal power flow problems using composite differential evolution integrating effective constrained handling techniques," *Scientific Reports*, vol. 14, no. 1, p. 6187, 2024.
- [12] A. A. Z. Diab, A. M. Abdelhamid, and H. M. Sultan, "Comprehensive analysis of optimal power flow using recent metaheuristic algorithms," *Scientific Reports*, vol. 14, no. 1, p. 13422, 2024.
- [13] G. S. Misyris, A. Venzke, and S. Chatzivasileiadis, "Physics-informed neural networks for power systems," in *2020 IEEE Power & Energy Society General Meeting (PESGM)*. IEEE, 2020, pp. 1–5.
- [14] D. Owerko, F. Gama, and A. Ribeiro, "Optimal power flow using graph neural networks," in *ICASSP 2020-2020 IEEE International Conference on Acoustics, Speech and Signal Processing (ICASSP)*. IEEE, 2020, pp. 5930–5934.
- [15] S. Zeng, A. Kody, Y. Kim, K. Kim, and D. K. Molzahn, "A reinforcement learning approach to parameter selection for distributed optimal power flow," *Electric Power Systems Research*, vol. 212, p. 108546, 2022.
- [16] M. R. Narimani, D. K. Molzahn, D. Wu, and M. L. Crow, "Empirical investigation of non-convexities in optimal power flow problems," in *2018 Annual American Control Conference (ACC)*. IEEE, 2018, pp. 3847–3854.
- [17] M. Chatzos, F. Fioretto, T. W. Mak, and P. Van Hentenryck, "High-fidelity machine learning approximations of large-scale optimal power flow," *arXiv preprint arXiv:2006.16356*, 2020.
- [18] F. Feng, Y. Zhou, and P. Zhang, "Quantum power flow," *IEEE Transactions on Power Systems*, vol. 36, no. 4, pp. 3810–3812, 2021.
- [19] F. Feng, Y.-F. Zhou, and P. Zhang, "Noise-resilient quantum power flow," *iEnergy*, vol. 2, no. 1, pp. 63–70, 2023.
- [20] Z. Kaseb, M. Möller, G. T. Balducci, P. Palensky, and P. P. Vergara, "Quantum neural networks for power flow analysis," *Electric Power Systems Research*, vol. 235, p. 110677, 2024.
- [21] P. Pareek, A. Jayakumar, C. Coffrin, and S. Misra, "Demystifying quantum power flow: Unveiling the limits of practical quantum advantage," *arXiv preprint arXiv:2402.08617*, 2024.
- [22] B. Sævarsson, S. Chatzivasileiadis, H. Jóhannsson, and J. Østergaard, "Quantum computing for power flow algorithms: Testing on real quantum computers," *arXiv preprint arXiv:2204.14028*, 2022.
- [23] J. Liu, H. Zheng, M. Hanada, K. Setia, and D. Wu, "Quantum power flows: From theory to practice," *Quantum Machine Intelligence*, vol. 6, no. 2, p. 55, 2024.
- [24] M. R. Magar, D. Pandit, D. Nguyen, and N. Nguyen, "Dc optimal power flow in unit commitment using quantum computing: An admm approach," in *2024 56th North American Power Symposium (NAPS)*. IEEE, 2023, pp. 1–6.
- [25] B. Boddu, M. H. Krishna, N. Kumar, N. Singh, A. M. Lafta *et al.*, "Quantum computing approaches to optimal power flow in complex grid networks," in *2023 International Conference on Power Energy, Environment & Intelligent Control (PEEIC)*. IEEE, 2023, pp. 752–756.
- [26] F. Amani, R. Mahroo, and A. Kargarian, "Quantum-enhanced dc optimal power flow," in *2023 IEEE Texas Power and Energy Conference (TPEC)*. IEEE, 2023, pp. 1–6.
- [27] C. C. McGeoch, *Adiabatic quantum computation and quantum annealing: Theory and practice*. Springer Nature, 2022.
- [28] P. Halfmann, P. Holzer, K. Plociennik, and M. Trebing, "A quantum computing approach for the unit commitment problem," in *International conference on operations research*. Springer, 2022, pp. 113–120.
- [29] E. Pelofske, A. Bärtzchi, and S. Eidenbenz, "Short-depth qaoa circuits and quantum annealing on higher-order ising models," *npj Quantum Information*, vol. 10, no. 1, p. 30, 2024.
- [30] S. F. Hafshejani, M. M. Uddin, D. Neufeld, D. Gaur, and R. Benkoczi, "Quantum algorithms for optimal power flow," *arXiv preprint arXiv:2412.06177*, 2024.
- [31] T. Morstyn, "Annealing-based quantum computing for combinatorial optimal power flow," *IEEE Transactions on Smart Grid*, vol. 14, no. 2, pp. 1093–1102, 2022.
- [32] Z. Kaseb, M. Möller, P. P. Vergara, and P. Palensky, "Power flow analysis using quantum and digital annealers: a discrete combinatorial optimization approach," *Scientific Reports*, vol. 14, no. 1, p. 23216, 2024.
- [33] R. Wagle, G. Tricarico, A. F. S. Melo, V. Rosero-Morillo, A. Shukla, F. Gonzalez-Longatt *et al.*, "Real-time cyber-physical power system testbed for optimal power flow study using co-simulation framework," *IEEE Access*, vol. 12, pp. 150 914–150 929, 2024.
- [34] R. Wagle, P. Sharma, C. Sharma, M. Amin, J. L. Rueda, and F. Gonzalez-Longatt, "Optimal power flow-based reactive power control in smart distribution network using real-time cyber-physical co-simulation framework," *IET Generation, Transmission & Distribution*, vol. 17, no. 20, pp. 4489–4502, 2023.
- [35] S. Chanda, M. Mohanpurkar, and R. Hovsapian, "Architecture for quantum-in-the loop real-time simulations for designing resilient smart grids," in *2023 13th International Symposium on Advanced Topics in Electrical Engineering (ATEE)*. IEEE, 2023, pp. 1–6.

¹<https://en-portal.research.global.fujitsu.com/kozuchi>